Biochemical and Biophysical Research Communications 378 (2009) 51–56

Contents lists available at ScienceDirect

Biochemical and Biophysical Research Communications

journal homepage: www.elsevier.com/locate/ybbrc

Mutational analysis of a signaling aptamer suggests a mechanism for ligand-triggered structure-switching

Jeffrey E. Vandenengel, Daniel P. Morse *

Department of Chemistry, United States Naval Academy, 572M Holloway Road, Annapolis, MD 21402, USA

ARTICLE INFO

Article history:
Received 29 October 2008
Available online 21 November 2008

Keywords:
Aptamer
Structure-switching
In vitro selection
RNA
Mutagenesis
Mechanism

ABSTRACT

Structure-switching signaling aptamers are nucleic acids that change shape upon binding to a specific ligand. Previously, we applied a new *in vitro* selection strategy to isolate structure-switching RNA aptamers responsive to the aminoglycoside antibiotic tobramycin. Here, we report the results of mutational analysis, secondary structure modeling, and ligand-specificity studies that suggest a mechanism for tobramycin-triggered structure switching.

Published by Elsevier Inc.

Structure-switching signaling aptamers are RNA or DNA molecules, produced by *in vitro* selection, that undergo a conformational change upon binding to a specific ligand. Aptamers of this type can function as highly sensitive and specific probes for the detection and quantification of the ligand [1]. Riboswitches are naturally-occurring RNA elements found in the untranslated regions of messenger RNAs that regulate gene expression through metabolite-triggered structure-switching [2–4]. Due to the large number of potential applications for signaling aptamers and artificial riboswitches [5], there is great interest in their efficient production and in understanding the mechanisms by which they detect their ligands.

We recently reported a new *in vitro* selection procedure that simultaneously selected for the two properties required of signaling aptamers: specific ligand binding and structure-switching [6]. We used the method to isolate RNA aptamers that change conformation upon binding to the aminoglycoside antibiotic tobramycin. Similar strategies have been reported for the selection of aptamers that respond to ATP/GTP and to zinc ion [7–8].

Here, we report the isolation of a tobramycin-signaling aptamer with increased sensitivity and the results of mutational analysis and ligand-specificity studies. The results pointed to the likely tobramycin binding site and suggested that the tobramycin-triggered conformational change involved the disruption of a pseudoknot followed by a simple rearrangement of the secondary structure.

Materials and methods

Fluorescence measurements. Fluorescence measurements were performed with a Modulus fluorometer (Turner Biosystems) in raw fluorescence mode using the blue fluorescence optical kit.

Oligonucleotides and RNA synthesis. Oligonucleotides were obtained from Integrated DNA Technologies, Inc (IDT).

DM002 (5′-CATTCC-3′-biotin; biotin was attached via a 9 carbon spacer).

DM003 (5′-GATAATACGACTCACTATAGGAATGGATCCACATCTACGA-3′).

DM004 (5′-AAGCTTCGTCAAGTCTGCAGTGAA-3′).

JV002 (5′-GAATGGATCCACATCTACGAAggctttgaaggtgagaccgtgcaaatgaggatggtgtggatgattagggttgctggttTTCACTGCAGACTTGACGAA-3′). Lower case letters represent a partially randomized region. For each position within the randomized region, phosphoamidites were hand-mixed such that 79% of molecules contained the given nucleotide and 21% contained one of the other three nucleotides (each with a 7% probability of occurrence). Flanking constant regions (uppercase) provided priming sites. Given sequence corresponds to previously selected tobramycin-signaling aptamer called 14-2 RNA [6].

DMA415256 (5′-GGATCCACATCTACGAAGGCTTTGAAGGTGAGACCATGCAAATGAGAATGATGTGGATGATTAGGGTTGCTGGTTTTCACTGCAGACTTG-3′).

Transcription templates were generated by PCR using JV002 or DMA415256 as templates and DM003 and DM004 as primers. DM003 included a T7 RNA polymerase promoter. RNA was synthesized by *in vitro* transcription with T7 RNA polymerase and labeled

* Corresponding author. Fax: +1 410 293 2218.
E-mail address: morse@usna.edu (D.P. Morse).

0006-291X/$ - see front matter Published by Elsevier Inc.
doi:10.1016/j.bbrc.2008.10.180

with fluorescein at their 3′-ends. PCR, transcription, and labeling were performed as previously described [6]. To introduce mutations during PCR, sequence changes were incorporated into the primers (DM003 and DM004) or into the template (DMA415256).

In vitro selection and structure-switching assays. Selection was performed as previously described [6]. The procedure for structure-switching assays is outlined in Fig. 1. It was identical to the method used for *in vitro* selection except reactions were performed on a smaller scale. DM002, a 6-base, biotinylated DNA oligonucleotide was immobilized by binding to streptavidin-coated magnetic beads. Each fluorescein-labeled RNA aptamer was bound to the beads by base-pairing with DM002. 50 μL RNA binding reactions contained: 4 μg (~115 pmol) of RNA, 0.25 mg of DM002 beads (~150 pmol DM002) and binding buffer (50 mM Tris, pH 7.4, 500 mM NaCl). RNA binding reactions were incubated overnight at 4 °C. Beads were rinsed quickly four times and washed twice for 30 min with 50 μL of binding buffer at 4 °C. RNA was eluted by incubating beads for 30 min at 4 °C with 50 μL of binding buffer containing antibiotic. After each step, beads were captured with a magnetic stand to allow for solution exchange. After the second 30 min wash and after the elution step, beads were captured and 40 μL of the supernatant was transferred to a tube containing 60 μL of binding buffer. RNA that remained bound to the beads was released by incubating beads at 65 °C for 5 min. Beads were again captured and 40 μL of supernatant was transferred to a tube containing 60 μL of binding buffer. The amount of RNA in each of the three collected fractions (wash, elution, and 65 °C incubation) was determined by measuring fluorescence intensities. The total amount of RNA originally bound to the DM002 beads was calculated as total amount of RNA present in the three collected fractions. Net efficiency of RNA elution (% elution) with antibiotic was calculated by subtracting percentage of bound RNA eluted with buffer during second 30 min wash from percentage of RNA eluted with ligand. Each experiment was repeated at least four times and two-tailed *t*-tests were used to compare averages. Microsoft Excel was used to perform *t*-tests and to calculate *p*-values.

Secondary structure predictions. Secondary structure predictions at 4 °C were made using Mfold version 2.3 (http://mfold.bioinfo.rpi.edu/cgi-bin/rna-form1-2.3.cgi [9–10]). To model the secondary structure of the bead-bound form of the RNA, the DM002 sequence, CAUUCC (with U replacing T) was appended to the 3′-end of the RNA and forced to pair with the 5′-end.

Results and discussion

A tobramcyin-signaling aptamer with improved sensitivity and no loss of ligand-specificity

Our original *in vitro* selection experiment produced two RNA aptamers (14-1 RNA and 14-2 RNA) that responded to tobramycin with minimum detection limits of 200 and 30 μM tobramycin, respectively [6]. In an attempt to generate variants with improved tobramycin sensitivity, we partially randomized the central 59 (out of 104) nucleotides of the 14-2 RNA sequence and repeated the selection. Alignment of 20 cDNA sequences from the 14th round of selection revealed that positions 37, 41, 52, and 56 showed a strong tendency toward G-to-A substitutions (Supplement 1). The alignment also revealed that, in all 20 sequences, 36 of the 59 nucleotides were identical to those present in 14-2 RNA. The region from positions 42–76 was particularly rich in invariant nucleotides suggesting a central role in tobramycin-signaling.

Structure switching assays (outlined in Fig. 1) showed that G-to-A substitutions at positions 41, 52, or 56 improved structure switching efficiency in the presence of 20 μM tobramycin (Supplement 2). Structure-switching efficiency was measured as the fraction of bound RNA that could be eluted from an immobilized complementary oligonucleotide (see Fig. 1). However, substitution at position 37 reduced the efficiency. This "false positive" may simply be an artifact of sequencing only 20 molecules from a large RNA pool. The effects of G-to-A substitutions at positions 41, 52, and 56 were additive. The elution efficiency of each of the three possible double mutants was greater than that of the single mutants and the efficiency of the triple mutant (A415256 RNA) was greater still.

The elution efficiencies of the triple mutant (A415256 RNA) and the original tobramycin aptamer (14-2 RNA) were measured as a function of tobramycin concentration in order to determine the minimum reproducibly detectable concentration of tobramycin (Supplement 2). A415256 RNA exhibited a 5-fold lower minimum detection limit than 14-2 RNA (2 μM vs. 10 μM tobramycin).

We analyzed the ligand-specificity of the two RNAs by measuring their elution efficiencies in the presence of a variety of aminoglycoside antibiotics at a concentration of 30 μM (concentration of tobramycin at about ½ the maximum elution efficiency). The two RNAs displayed similar ligand preferences. Both 14-2 and A415256 RNA could detect 30 μM kanamycin B but with a significantly decreased efficiency compared to 30 μM tobramycin ($p = 8 \times 10^{-4}$ and 9×10^{-5}, respectively). The RNAs could barely detect 30 μM kanamycin A and neither RNA responded at all to amikacin or paromomycin (Supplement 3).

Structure–function studies suggest a model for tobramycin-triggered structure switching

Comparative sequence analysis of natural or artificially generated variants is a well-established method for detecting functionally-important base-paired regions in RNA [11–14]. Mutations that disrupt such pairings interfere with RNA function. If the structure but not the sequence is important for function, then function will be restored by compensatory mutations that restore pairing.

In order to generate variants for our structure–function studies, we performed site-directed mutagenesis on A415256 RNA. To guide our mutational analysis, we generated candidate secondary structures for A415256 RNA using Mfold (http://mfold.bioinfo.rpi.edu/cgi-bin/rna-form1-2.3.cgi [9–10]). The most stable predicted fold at 4 °C for A415256 RNA is shown in Fig. 2A (soluble form). Positions 37, 41, 52, and 56 are highlighted in light blue. To model the secondary structure of the bead-bound form of the RNA, the DM002 sequence, CAUUCC (with U replacing T) was appended to the 3′-end of the RNA and forced to pair with the 5′-end (Fig. 2A; bead-bound form). If the structural models are correct, then RNA elution would involve a simple conformational change in which the 5′-end detaches from DM002 and folds back on itself to form

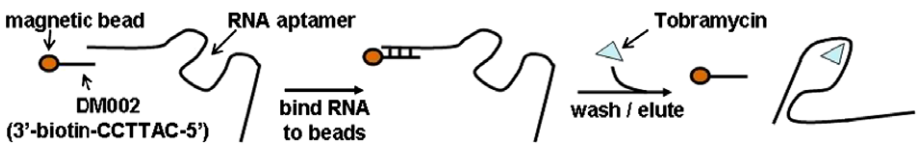

Fig. 1. Outline of structure switching assay. Fluorescein-labeled RNA was bound to streptavidin-coated magnetic beads by base-pairing with an immobilized oligonucleotide (DM002). The beads were washed with buffer and RNA was eluted with tobramycin.

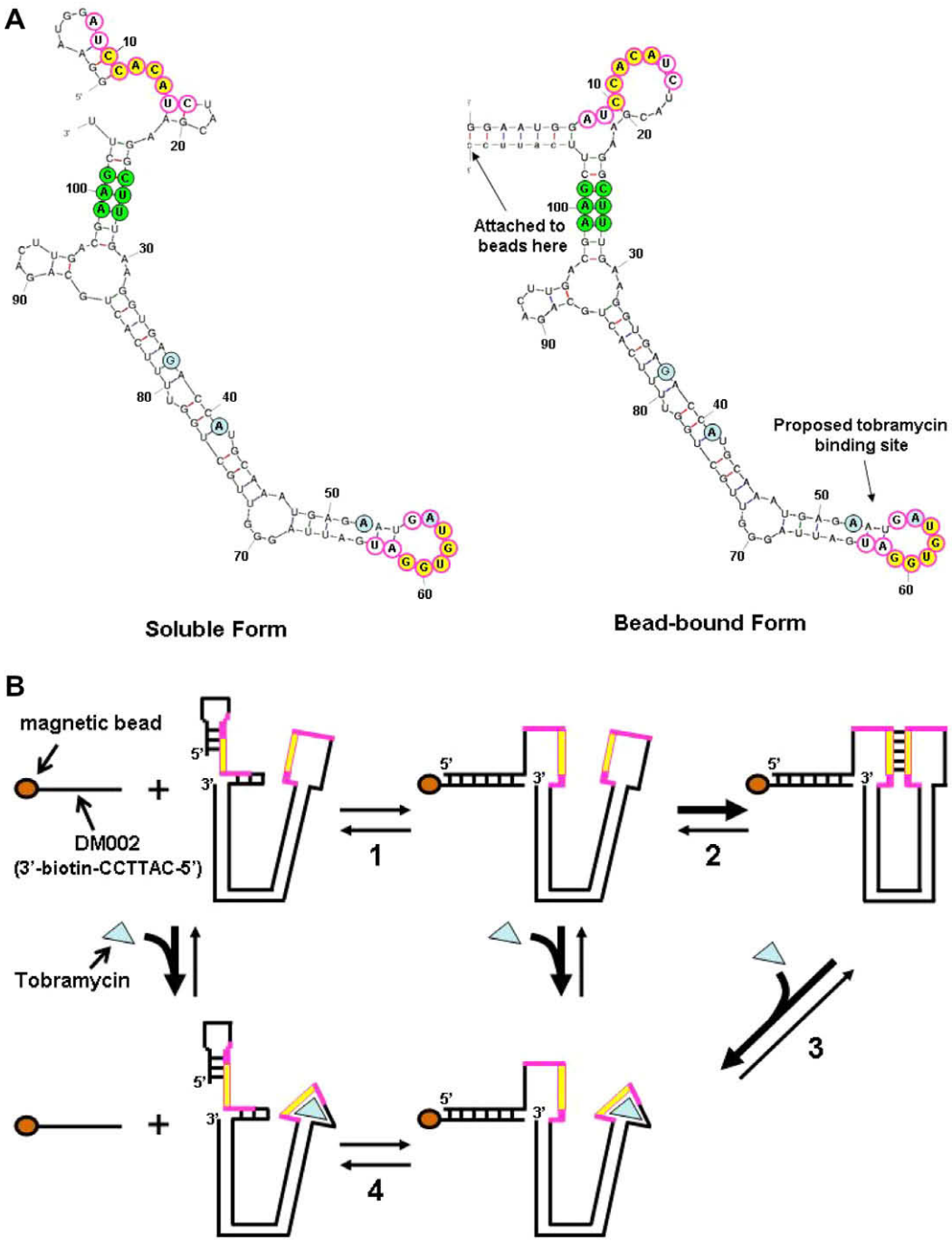

Fig. 2. (A) Mfold-generated secondary structure predictions. To predict the structure of the bead-bound form, the sequence of DM002 (CATTCC) was added to the 3′-end of the RNA. This sequence is shown in lower case letters with U substituted for T. Bases highlighted in blue indicate sites at which G-to-A substitutions decreased (position 37) or increased (positions 41, 52, 56) elution efficiency. The two groups of bases circled in magenta (8–16 and 55–63) are complementary and potentially pair to form a pseudoknot. Bases highlighted in green and yellow indicate base pairs supported by mutational analysis. The site of DM002 attachment to the beads and the proposed tobramycin binding site (stem-loop formed by nucleotides 48–68) are indicated. (B) Model for the mechanism of tobramycin-triggered structure switching. The bead-bound form of the RNA is stabilized by the formation of a pseudoknot (reactions 1 and 2). Tobramycin binding disrupts the pseudoknot causing the RNA to switch to the soluble form and elute from the beads (reactions 3 and 4). Base pairs shown explicitly are those that rearrange during the conformational changes. Magenta and yellow segments indicate the complementary bases that potentially pair to form a pseudoknot.

the two small hairpins present in the soluble form, leaving the rest of the secondary structure unchanged.

As a first test of the structural models, we used mutational analysis to gain evidence for the pairing of nucleotides 25–27 (CUU) with nucleotides 99–101 (AAG). These triplets are highlighted in green in Fig. 2A. We synthesized three variants of A415256 RNA and measured their elution efficiencies with 30 μM tobramycin. The three putative base pairs were disrupted in variants 1 and 2, and the potential for base-pairing was restored in variant 3. The results of the experiment are shown in Fig. 3B. The elution efficiencies of both variants 1 and 2 were about six times lower than that of A415256 RNA ($p = 0.0005$ and 0.0004, respectively) while the elution efficiency of variant 3 was nearly identical to that of A415256 RNA. These results support the existence of the C25-

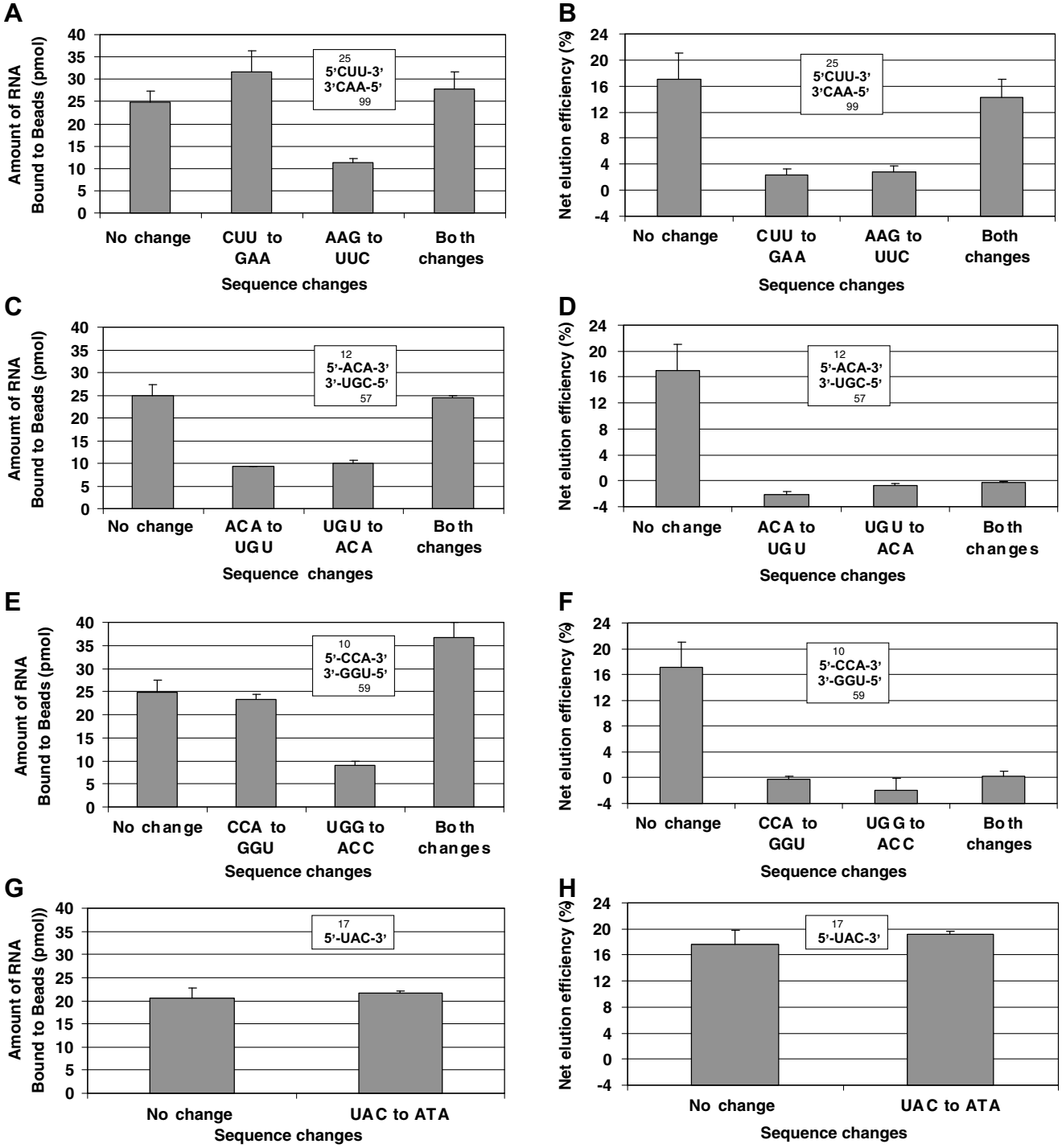

Fig. 3. Mutational analysis of A415256 RNA structure and function. Legends show the regions that were mutated. (A), (C), (E), (G) Amount of RNA initially bound to DM002 beads. (B), (D), (F), (G) Elution efficiency of RNAs with 30 μM tobramycin. In (A) through (F), the results for the RNA with no sequence changes are the average of the same set of six experiments. All other results are the average of four experiments. Error bars represent standard deviations.

U27/A99-G101 duplex and, by extension, the existence of the entire G23-G29/C97-U103 helix.

Nucleotides 8–16 in A414256 RNA are complementary to nucleotides 55–63 (magenta circles in Fig. 2A). In the bead-bound form of the RNA, both of these regions lie mostly within single-stranded loops so they have the potential to pair and form a pseudoknot. In contrast, the soluble form of the RNA sequesters much of the 8–16 region within two small hairpins. These observations suggest a model for the mechanism of tobramycin-triggered structure switching (Fig. 2B). We propose that pseudoknot formation stabilizes the bead-bound form of the RNA (reactions 1 and 2 in Fig. 2B) and that tobramycin binding destabilizes the pseudoknot, triggering a switch from the bead-bound form to the soluble form (reactions 3 and 4 in Fig. 2B). If the proposed mechanism is correct, mutations that disrupt the putative pseudoknot should have two effects: the amount of RNA that initially binds to the beads should decrease; and tobramycin should have little or no effect on the equilibrium between the bead-bound and soluble forms of the RNA.

To test these ideas, we mutated nucleotides involved in formation of the pseudoknot. For each variant, we measured the amount

of RNA initially bound to the beads and the elution efficiency with 30 μM tobramycin. We generated variants that either eliminated or retained the potential for pairing between ACA (nucleotides 12–14) and UGU (nucleotides 57–59). These triplets were chosen because they were predicted to be single-stranded in both forms of the RNA (highlighted in yellow in Fig. 2A). Therefore, the mutations were unlikely to significantly alter the secondary structures. Disruption of the pairings reduced the amount of RNA that bound to the beads by more than 50% ($p = 1 \times 10^{-3}$ and 3×10^{-4}, respectively), but when the two substitutions were combined, normal binding to the beads was restored (Fig. 3C). These results support the existence of the pseudoknot and are consistent with the idea that the pseudoknot stabilizes the bead-bound form of the RNA. As predicted, disruption of the ACA/UGU pairing completely eliminated the ability of the RNA to elute with 30 μM tobramycin. However, restoring the potential for pairing did not restore this function (Fig. 3D). Since tobramycin is proposed to disrupt the pseudoknot, a likely explanation for these results is that the mutations in variant 1 or 2 (or both) destroy the tobramycin binding site.

In the next experiment, we mutated nucleotides 10–12 (CCA) and nucleotides 59–61 (UGG). The UGG triplet is predicted to be single-stranded in both forms of the RNA but the CC of the CCA triplet forms part of a small hairpin in the soluble form (highlighted in yellow in Fig. 2A). Interestingly, the effects on RNA binding (Fig. 3E) were not the same as in the previous experiment, providing further support for our proposed mechanism. Although changing UGG (59–61) to ACC greatly reduced RNA binding, changing CCA (10–12) to GGU had no measurable effect. Importantly, when both substitutions were made, RNA binding increased significantly ($p = 6 \times 10^{-4}$). As in the previous experiment, poor RNA binding due to the UGG to ACC change can be explained by disruption of the pseudoknot and consequent destabilization of the bead-bound form of the RNA. Why did the CCA to GGU change have no effect on RNA binding to the beads despite disrupting the pseudoknot? This mutation destabilizes the short hairpin that sequesters the 5′-end of the RNA in the soluble form. Mfold predicts that the bead-bound form of this mutant folds into a significantly more stable secondary structure (not shown). The increased stability of the bead-bound form relative to the soluble form apparently compensates for the loss of the pseudoknot and allows the RNA to bind stably to the beads. The combined effects of a more stable secondary structure in the bead-bound form and restoring the pseudoknot (which further stabilizes the bead-bound form) explain why the double substitution increased the amount of RNA binding to the beads. As in the previous experiment, all three variants eliminated tobramycin responsiveness (Fig. 3F).

The results in Fig. 3A show that destabilization of the 23–29/97–103 helix affected RNA binding to the beads. Changing CUU (nucleotides 25–27) to GAA significantly increased RNA binding ($p = 0.02$) while changing AAG (nucleotides 99–101) to UUC reduced binding to the beads by more than 50% ($p = 1 \times 10^{-5}$). When both changes were made, the amount of RNA bound to the beads was indistinguishable from that of unmutated A415256 RNA. These results are likely due to changes in the local secondary structure that indirectly alter the stability of the pseudoknot. Each mutation that disrupted the 23–29/97–103 helix significantly changed the predicted secondary structures in the region of the helix (not shown). This probably affects the ability of the complementary loops to approach each other with the correct geometry for pseudoknot formation. When pairing is restored, the secondary structures are predicted to be identical to those shown in Fig. 2A. Consequently, RNA binding to the beads returns to normal. These results highlight the importance of the structure and flexibility of the long imperfect helix that connects the complementary loops. Changes in the structure/stability of the connector may explain the effects of changing G-to-A at positions 37 and 41 (highlighted in light blue in Fig. 2A).

As a final test of the model, UAC at positions 17–19 was changed to AUA. This triplet is predicted to lie in a single-stranded region in both forms of the RNA and it does not participate in pseudoknot formation (Fig. 2A). As expected, this change had no effect on either RNA binding to the beads or elution efficiency (Fig. 3G and H).

Mutational analysis and specificity studies reveal the likely tobramycin binding site

Our data support the idea that tobramycin triggers a conformational change in our aptamer by disrupting a pseudoknot (Fig. 2B). This leads to two questions: Where does tobramycin bind and why does this binding disrupt the pseudoknot? Based on the results of our mutational analysis and specificity studies, and considering the known properties of other tobramycin aptamers, we propose that the stem-loop formed by nucleotides 48–68 in our aptamer is the tobramycin binding site (Fig. 2A and B). We propose that there is a single specific tobramycin binding site (rather than multiple binding sites) because the dependence of structure-switching efficiency on tobramycin concentration fit well to simple hyperbolic binding curves with a single saturable binding site [6].

There are some striking similarities between our proposed tobramycin binding site and two previously selected tobramycin aptamers (designated aptamers I and II). Solution structures of aptamers I and II bound to tobramycin revealed the architectural principles that allowed tobramycin to bind with high affinity and specificity [15–16]. These aptamers form stem-loop structures that are 25–27 nucleotides long. Tobramycin binds between a flipped out base in the loop and the floor of the major groove of the A-form helical stem. In order to accommodate tobramycin, the major groove is widened by a bulged adenosine in aptamer I and by non-Watson Crick pairs in aptamer II. Importantly, the loop portion of the RNAs becomes highly structured upon tobramycin binding. In both aptamers, the A-form helix continues into the loop region and the loop folds down over the top of the bound tobramycin completing a binding pocket in which the shape and charge are highly complementary to those of tobramycin. The structure of the aptamer II-tobramycin complex shows that several residues in the loop region may form hydrogen bonds to tobramycin.

The specificity of our tobramycin-signaling aptamers closely parallels that of aptamer II (relative binding affinities: tobramycin > kanamycin B ≫ kanamycin A), suggesting that these RNAs bind to tobramycin in a similar fashion [16–17]. Not all RNAs that bind to tobramycin exhibit the same ligand preferences. For example, the A-site in 16S rRNA is a physiological target of many different aminoglycosides including tobramycin. The relatively low selectivity of this RNA can be explained by the details of the ligand–RNA contacts which differ significantly from those seen in aptamers I and II [18].

The results of our mutational analysis and specificity studies are consistent with the idea that tobramycin binds to the stem-loop formed by nucleotides 48–68 (Fig. 2A and B). This hypothesis explains why mutations in the loop eliminated tobramycin responsiveness (Fig. 3D and F) and suggests a simple and compelling mechanism for tobramycin-triggered structure switching. The loop directly participates in pseudoknot formation and tobramycin would disrupt the pseudoknot if, as suggested by our specificity experiments, its mode of binding is similar to that seen in aptamers I and II. Sequence alignment of the RNAs that survived selection showed that nucleotides 42–76 contained a striking number of invariant nucleotides suggesting that the stem-loop plays a particularly important role in aptamer function (Supplement 1). The

stem includes non-Watson-Crick pairs (G51-A65 and A52-G64) that widen the major groove as seen in the solution structure of aptamer II. There was strong selection for a G-to-A change at position 52 which preserved the purine-purine mismatch with G64 and resulted in improved elution efficiency with tobramycin (Supplements 1 and 2). The absence of C or U at this position in the selected RNA pool suggests that it is important to maintain the mismatch. Among the selected G-to-A changes, the one at position 56 was enriched to the greatest extent and had the greatest effect on elution efficiency (Supplements 1 and 2). Position 56 lies in the loop and the G-to-A change stabilizes the pseudoknot because it changes a G-U pair to a more stable A-U pair (Fig. 2A). Improved elution efficiency and the consequent enrichment of A at positions 52 and 56 during *in vitro* selection may be due to increased affinity for tobramycin.

Our model for the mechanism of tobramycin-triggered structure switching makes a number of readily testable predictions. Enzymatic and chemical probing of the RNA structure can test whether or not the proposed pseudoknot forms and whether its stability is influenced by tobramycin or mutation. Our proposal that nucleotides 48–68 constitute the tobramycin binding site and that A to G changes at positions 52 and 56 alter the affinity for tobramycin can be tested by performing binding assays with truncated RNAs. These experiments are currently underway in our laboratory.

Acknowledgments

Thanks to Virginia Smith, Jamie Schlessman, and Shirley Lin for critical reading of the manuscript. This work was supported by the National Institutes of Health [NS052753 to D.P.M.]; the Office of Naval Research via the Naval Academy Trident Scholar Program [N0001408WR40063 to J.E.V.]; and the Chemistry Department of the US Naval Academy.

Appendix A. Supplementary data

Supplementary data associated with this article can be found, in the online version, at doi:10.1016/j.bbrc.2008.10.180.

References

[1] R. Nutiu, Y. Li, Structure-switching signaling aptamers: transducing molecular recognition into fluorescence signaling, Chemistry 10 (2004) 1868–1876.
[2] T.E. Edwards, D.J. Klein, A.R. Ferre-D'Amare, Riboswitches: small-molecule recognition by gene regulatory RNAs, Curr. Opin. Struct. Biol. 17 (2007) 273–279.
[3] R.K. Montange, R.T. Batey, Riboswitches: emerging themes in RNA structure and function, Annu. Rev. Biophys. 37 (2008) 117–133.
[4] C.A. Wakeman, W.C. Winkler, C.E. Dann 3rd, Structural features of metabolite-sensing riboswitches, Trends Biochem. Sci. 32 (2007) 415–424.
[5] B. Suess, J.E. Weigand, Engineered riboswitches: overview, problems and trends, RNA Biol. 5 (2008) 24–29.
[6] D.P. Morse, Direct selection of RNA beacon aptamers, Biochem. Biophys. Res. Commun. 359 (2007) 94–101.
[7] R. Nutiu, Y. Li, In vitro selection of structure-switching signaling aptamers, Angew. Chem. Int. Ed. Engl. 44 (2005) 1061–1065.
[8] M. Rajendran, A.D. Ellington, Selection of fluorescent aptamer beacons that light up in the presence of zinc, Anal. Bioanal. Chem. 390 (2008) 1067–1075.
[9] A.E. Walter, D.H. Turner, J. Kim, M.H. Lyttle, P. Muller, D.H. Mathews, M. Zuker, Coaxial stacking of helixes enhances binding of oligoribonucleotides and improves predictions of RNA folding, Proc. Natl. Acad. Sci. USA 91 (1994) 9218–9222.
[10] M. Zuker, Mfold web server for nucleic acid folding and hybridization prediction, Nucleic Acids Res. 31 (2003) 3406–3415.
[11] C.R. Woese, L.J. Magrum, R. Gupta, R.B. Siegel, D.A. Stahl, J. Kop, N. Crawford, J. Brosius, R. Gutell, J.J. Hogan, H.F. Noller, Secondary structure model for bacterial 16S ribosomal RNA: phylogenetic, enzymatic and chemical evidence, Nucleic Acids Res. 8 (1980) 2275–2293.
[12] R.R. Gutell, H.F. Noller, C.R. Woese, Higher order structure in ribosomal RNA, EMBO J. 5 (1986) 1111–1113.
[13] R.R. Gutell, J.C. Lee, J.J. Cannone, The accuracy of ribosomal RNA comparative structure models, Curr. Opin. Struct. Biol. 12 (2002) 301–310.
[14] S. Engelen, F. Tahi, Predicting RNA secondary structure by the comparative approach: how to select the homologous sequences, BMC Bioinformatics 8 (2007) 464.
[15] L. Jiang, A.K. Suri, R. Fiala, D.J. Patel, Saccharide-RNA recognition in an aminoglycoside antibiotic-RNA aptamer complex, Chem. Biol. 4 (1997) 35–50.
[16] L. Jiang, D.J. Patel, Solution structure of the tobramycin-RNA aptamer complex, Nat. Struct. Biol. 5 (1998) 769–774.
[17] S.H. Verhelst, P.J. Michiels, G.A. van der Marel, C.A. van Boeckel, J.H. van Boom, Surface plasmon resonance evaluation of various aminoglycoside-RNA hairpin interactions reveals low degree of selectivity, Chembiochem 5 (2004) 937–942.
[18] D.H. Ryu, R.R. Rando, Aminoglycoside binding to human and bacterial A-Site rRNA decoding region constructs, Bioorg. Med. Chem. 9 (2001) 2601–2608.